Surface-Dependent Photocatalytic and Biological Activities of Ag_2CrO_4: Integration of Experiment and Simulation

Marcelo Assis[a], Camila Cristina de Foggi[a,e], Vinicius Teodoro[a], João Paulo de Campos da Costa[a], Carlos Eduardo Silva[b], Thaiane Robeldo[c], Priscila Fernanda Caperucci[a], Carlos Eduardo Vergani[d], Ricardo Carneiro Borra[c], Ivan Sorribes[e,†], Amanda Fernandes Gouveia[b,e], Miguel Angel San-Miguel[b], Juan Andrés[e,*], Elson Longo[a]

[a]CDMF, Universidade Federal de São Carlos – UFSCar, P.O. Box 676, 13565-905, São Carlos – SP, Brazil
[b]Institute of Chemistry, State University of Campinas, Unicamp, 13083-970, Campinas – SP, Brazil
[c]LIA, Laboratory of Applied Immunology, Department of Genetics and Evolution, Universidade Federal de São Carlos – UFSCar, P.O. Box 676, 13565-905, São Carlos – SP, Brazil
[d]FOAr-UNESP, Universidade Estadual Paulista, P.O. Box 1680, 14801903 Araraquara – SP, Brazil
[e]Department of Physical and Analytical Chemistry, Universitat Jaume I, 12071, Castelló, Spain
†Present address: Instituto de Tecnología Química, Universitat Politècnica de València-Consejo Superior de Investigaciones Científicas, Av. De los Naranjos, s/n, 46022, Valencia, Spain

ABSTRACT

In this work, we present a joint experimental and theoretical study towards unveiling the photocatalytic (photodegradation of Rhodamine B), the antifungal (towards *Candida glabrata*) and cytotoxicity (against the L929 cell line) of Ag_2CrO_4. X-ray diffraction, Rietveld refinements, micro-Raman, UV-Visible spectroscopies, and photoluminescence emissions have been employed to characterize the as-synthetized samples by a co-precipitation method in H_2O and NH_3 solvent. To complement and rationalize the experimental results, first-principles calculations have been performed within the framework of density functional theory. The crystal morphologies were characterized by field emission scanning electron microscopy images, while the Wulff construction, obtained by the calculated values of the surface energy, was employed to model and match the experimental images by tuning the relative stability of the exposed surfaces. This experimental and theoretical study provides a detailed understanding of the transformations of morphology and can aid in the development of the surface-dependent photocatalytic and biological activities of Ag_2CrO_4. We believe that our results offer new insights regarding the local coordination of superficial Ag and Cr cations on each exposed surface of the corresponding morphology, provided some general principles for material design, that dictate the properties of Ag_2CrO_4, a field that has so far remained unexplored.

Keywords: Ag_2CrO_4, Photocatalytic and biological activities, Morphology, Wulff construction, First-principles calculations.

1. Introduction

Silver chromate/molybdate/tungstate with the composition Ag_2MO_4, being M = Cr, Mo and W, respectively, are an important family of Ag-containing compounds. These materials present a wide range of technological applications as photoluminescent materials, photocatalysts, cathodes of lithium batteries, sensors, and so on [1–14]. Among them, a vast set of works has been performed on silver chromate (Ag_2CrO_4) due to its intrinsic and extrinsic properties, associated with its unique crystal and electronic structure, [14–25]. From an electronic point of view, the valence band (VB) is composed of the hybridization of Ag 4*d* and O 2*p* orbitals, while the conduction band (CB) is dominated by Cr 3*d* orbitals with a narrow band gap lower than 1.8 eV. The crystal structure is composed by elongated octahedral [AgO_6] clusters, distorted off-centered [AgO_4] clusters and tetrahedral [CrO_4] clusters, as building blocks at the orthorhombic unit cell (*Pnma* space group). This crystal structure, in which both Ag–O bond lengths and O–Ag–O bond angles, at both [AgO_6] and [AgO_4] clusters, present large values, is adequate to enhance the migration process of the photogenerated electrons (e') and holes $(h^{\bullet})$ [15,18,25–28].

Due to its practical applications, Ag_2CrO_4 has been extensively studied both experimentally [17,19,23,24,29–32] and theoretically [15,25–28,33,34]. These works highlight the importance of analyzing the crystal and the electronic structures to understand their properties, thus opening a doorway for developing this kind of material as visible-light-driven photocatalysts. However, its application as microbiological agents have not been investigated so far.

Our group is engaged in research projects devoted to the study of the structural, morphological, optical and photocatalytic properties of Ag_2CrO_4 microcrystals using a combination of theoretical calculations and experimental techniques [27,28]. As an extension of our research, in this article, Ag_2CrO_4 was synthetized by means of a co-precipitation (CP) method, in H_2O and NH_3 as a solvent, with the formation of homogeneous morphologies at different temperatures (30, 60 and 90 °C). The performances of the as-synthesized Ag_2CrO_4 samples for the degradation of Rhodamine B (RhB) are evaluated under visible-light irradiation. A systematic study of the antifungal activity (against *Candida glabrata* ATCC 2001, *C. glabrata*) and cytotoxicity (using the L929 cell line) were carried out in order to analyze the beneficial

implications of Ag_2CrO_4 in two of the most important bio-medical applications that directly impact the healthcare of human kind. To gain further insights, we performed density functional theory (DFT) calculations to complement the experimental results and rationalize the structure, electronic and optical properties of Ag_2CrO_4, and consequently, its photocatalytic, antifungal and antitumor performances.

Nowadays, the controlled synthesis of a great variety of semiconductors has been documented for an immense range of applications [35][36][37]. The novelty of the current work is in the study of the the morphology evolution systematically by varying solvent and temperature to better understand the complex behavior of the as-synthetized Ag_2CrO_4 samples. The remarkable aspect is the utilization of the first-principles calculations, on the basis of DFT, to complement and rationalize the experimental results. Based on the above considerations, in this study, we combine experimental and theoretical efforts to gather a comprehensive understanding of intrinsic properties of Ag_2CrO_4. To do so, the energetic, structural, electronic, morphological, and optical properties of Ag_2CrO_4 were analyzed by experimental techniques, with the major aspects being substantiated and further elucidated by DFT calculations.

Hence, we aim to achieve the following goals: (i) to determine the energy profiles associated with the morphology transformation processes at different temperatures, (ii) to clarify the critical role of the exposed surfaces and their singular chemical environments which govern the main properties of Ag_2CrO_4 material, (iii) to demonstrate, for first time, the antifungal activity and cytotoxicity of Ag_2CrO_4, (iv) to provide a deeper insight not only to disclose the nature of the mechanism but also to rationalize the origin of the photocatalytic, antifungal and cytotoxicity activities, and (v) to find a surface-dependent photocatalytic and biological activity relationship. Therefore, the projection of this work aims to extend the current efforts in terms of designing of multifunctional applications of Ag_2CrO_4 based materials with a unique morphology and potential for their use in biocide applications.

2. Experimental Section

Details of methods of synthesis, characterization techniques, and experimental and theoretical procedures are described in the Supplementary Information (SI). The analysis of the structural properties obtained from X-ray diffraction (XRD) with

Rietveld refinements, micro-Raman and UV-vis spectroscopies, and also the photoluminescence emissions related to the degree of order/disorder in the samples, are also presented in the SI.

3. Results and Discussion

3.1. Field Emission Scanning Electron Microscopy (FE-SEM) Analysis and Wulff Construction

It was observed in the literature that the morphology of the as-synthetized Ag_2CrO_4 microcrystals are dependent on the synthesis conditions, such as precursor physicochemical properties, temperature, pH, pressure, agitation, addition of surfactants, etc. Xu *et al.* [14] obtained Ag_2CrO_4 nanospheres with average diameter size of 30 nm, while Silva *et al.* [27] obtained several faceted polyhedra with an average size between 1 to 4 μm.

Fig. 1 displays the FE-SEM images of the samples synthetized by CP method using H_2O and NH_3 as a solvent. When the material was synthesized in H_2O at different temperatures, it was obtained a large amount of irregular morphologies (**Fig.1A-C**), while a morphological homogeneity is obtained for the samples synthetized with NH_3 (**Fig. 1D-F**) and the formation of rods in flower-like morphology (**Fig. 1D**) is observed.

Fig. 1. FE-SEM imagens of Ag_2CrO_4 powders obtained by CP method with H_2O as a solvent at A) 30, B) 60 and C) 90 °C and with NH_3 as a solvent at D) 30, E) 60 and F) 90 °C.

According to the size and width distribution on **Fig. 2A-C** for the samples synthetized with H_2O, as the temperature increases, both the average length (0.63, 0.72 and 0.73 μm, for 30, 60 and 90 °C, respectively) and width (0.52, 0.61 and 0.64 μm, for 30, 60 and 90 °C, respectively) of the obtained microcrystals increase, due to an enhancement of the effective collisions at higher temperatures. The samples synthetized with NH_3, a decrease in average length (12.37, 6.57 and 4.97 μm, for 30, 60 and 90 °C, respectively) and an increase of the average width were observed (2.40, 2.68 and 3.36 μm, for 30, 60 and 90 °C, respectively), due to the stabilization of the surfaces associated with the formation of the tip of the rods.

Fig. 2. Width and length distribution of Ag_2CrO_4 powders obtained by CP method with H_2O as a solvent at A-D) 30, B-E) 60 and C-F) 90 °C and with NH_3 as a solvent at G-J) 30, H-K) 60 and I-L) 90 °C.

In order to investigate the morphological evolution of the samples obtained with H_2O and NH_3, it was constructed the surfaces models from the Ag_2CrO_4 bulk structure from first-principles calculations. **Fig. 3** presents the surfaces modeled from DFT calculations for the Ag_2CrO_4 and their respective surface energy (E_{surf}) are reported in **Table 1**.

Fig. 3. Surfaces models of the Ag_2CrO_4 with their respective upper (l_1) and lower (l_2) terminations.

The (111) surfaces show the lowest values of E_{surf}, and among them, the l_2 terminated (bottom part of the slab) is energetically the most favorable. This stability is mainly due to the smaller relaxation energy of the l_2 compared to the l_1 termination, indicating that the rearrangement of the most external atoms plays the main contribution to the surface stability. For the others surfaces, the most favored terminations are represented in **Fig. 3**. As can be seen, the (001), (011) and (110) surfaces have high cleavage energy (E_{cut}), as a result of a significant number of broken bonds, i.e. large number of undercoordinated atoms as indicated by their relaxation energy (E_{rel}) values (**Table 1**).

Table 1. Studied surfaces, the corresponding terminations (l_i), the cleavage (E_{cut}), relaxation (E_{rel}), and surface (E_{surf}) energy values (in J/m^2), and number of atoms (NA) and their coordination number (CN) in the exposed surfaces.

From the calculated E_{surf} values and applying the Wulff construction it is possible to predict the equilibrium morphology for Ag_2CrO_4 crystals in *vacuum* using the VESTA program [38]. The ideal morphology, directly constructed from the computed E_{surf} values, is represented in the center of the **Fig. 4,** and it shows clearly the prevalence of the (111) surfaces with the lowest value of E_{surf} (0.90 J/m^2). In order to achieve the experimental morphologies, the surfaces stabilities were affected by increasing or decreasing some specific surfaces and the new E_{surf} values were indicated [39][40][41]. In **Fig. 4** we can select the experimental morphologies, obtained by the FE-SEM images that match with the theoretical morphologies using our procedure (morphologies 1 to 6).

Fig. 4. Theoretical and experimental morphologies obtained by tuning the values of E_{surf} for Ag_2CrO_4. The FE-SEM imagens for each sample is inserted for comparison purposes. Surface energy value in J/m^2.

According to the strategy used to achieve a specific morphology, it is possible to obtain the energy profiles, via the calculation of the polyhedron energy values ($E_{polyhedron}$),[11] that are capable to connect the ideal morphology with the experimental FE-SEM images obtained experimentally in both solvents at the three different temperatures. **Fig. 5** shows the different energy pathways, while in **Fig. 1** and **Table 2** are presented the E_{surf} and $E_{polyhedron}$ values for each morphology and also the contribution of the total surface area of each surface.

Fig. 5. Polyhedron energy profiles connecting the ideal and experimental morphologies (1-6).

Table 2. Surface energy values (E_{surf}, J/m^2), contribution of the surface area to the total area (C_i), and the polyhedron energy ($E_{polyhedron}$, J/m^2) for each crystal morphology of Ag_2CrO_4.

An analysis of the results presented in **Table 2** renders that the crystal morphology obtained at 30 °C in H_2O medium is the most stable (**Fig. 5**, morphology 1). The (001), (101), (011), and (110) surfaces are exposed, with prevalence of the first two surfaces. To obtain this morphology, the values of E_{surf} for these four surfaces need to be decreased, like shown in **Fig. 4**. The morphology obtained in NH_3 medium at the same temperature has a lower $E_{polyhedron}$ value than that computed for the ideal crystal morphology (**Fig. 5**, morphology 4). Therefore, their presence is associated to the decreases of the E_{surf} values due to surface/medium interactions in relation to that predicted *in vacuum*. Indeed, the predominant surfaces at this morphology are the (100) and (101) surfaces, and they require a decrease in the values of E_{surf}, 0.89 J/m^2 and 0.92 J/m^2, respectively. Simultaneously, the (010), (110) and (111) surfaces are destabilized by 1.65, 0.42 and 1.00 J/m^2, respectively. An inversion of the relative stability is observed in the samples obtained at 60 °C. The product synthesized in NH_3 (**Fig. 5**, morphology 5) has an $E_{polyhedron}$ value smaller than the one obtained in H_2O (**Fig. 5**, morphology 2). In the last case, the (010), (011) and (110) surfaces are the main components of the morphology with predominance of the first two surfaces and significant reduction of E_{surf} to 0.63 and 0.95 J/m^2 for both surfaces while the value of

E_{surf} of the (110) surface is maintained. Concomitantly, the E_{surf} value for the (100), (101) and (111) surfaces need to be increased to 3.65, 2.90 and 2.40 J/m^2, respectively. These changes result in a high $E_{polyhedron}$ value (1.05 J/m^2) indicating that this morphology occurs from a strong energy destabilization in relation to the ideal morphology.

For the synthesis in NH_3, we have a crystal morphology that exposes, predominantly, the (001), (011) and (111) surfaces. This morphology is obtained after a considerable reduction of the corresponding E_{surf} values at about 1.35 and 1.29 J/m^2, for (001) and (011) surfaces, respectively. The larger energetic stability of morphology 5 in relation to morphology 2 can be explained through the chemical composition of the clusters at the exposed surfaces. Additionally, it is worth to mention that the (011) surface is exposed in both morphologies and the most stable (111) surface is present only in the morphology 5. At 90 °C, similarly to described for the samples obtained at 30 °C, the crystal morphology in H_2O is the most energetically stable, and as can be seen in the **Fig. 5** (morphology 3), the (010), (001) and (011) surfaces are not present, while the crystal morphology of 6 is widely dominated by the (001) and (101) surfaces with a smaller contribution of the (100), (011) and (110) surfaces and present the highest $E_{polyhedron}$ among the morphologies obtained in NH_3.

The theoretical morphologies obtained from the calculated E_{surf} values by using the Wulff construction for the Ag_2CrO_4 samples, synthesized in H_2O and NH_3 were formed by different combination of surfaces and, from the theoretical study, it is possible to disclose the nature of the clusters of Ag and Cr atoms, i.e. local coordinations present in each surfaces of all morphologies. In this way, we can also calculate the broken bonds density (D_b) which is the result of the ratio of the number of broken bonds (N_b) by the area of the surface (A). Using the Kröger-Vink notation[42] to assign the neutral oxygen vacancy as V_o^x, the clusters of the undercoordinated Ag and Cr atoms at the top of all surfaces can be written as illustrated on **Fig. 6**. At this point, it is important to remark the geometry and electronic structure of the models used to represent the exposed surfaces are responsible of the chemical/physical properties of the semiconductors.

Fig. 6. Surface models for the Ag_2CrO_4 structure where the Ag and Cr clusters are highlighted. V_o^x corresponds to a neutral oxygen vacancy. The values of D_b and E_{surf} are also presented.

As can be seen in **Fig. 6**, the undercoordinated $[AgO_3 \cdot 3V_o^x]$ clusters are present in all surfaces and the (001) and (101) surfaces are constituted by only this kind of undercoordinated cluster. By the other side, the undercoordinated $[AgO_4 \cdot 2V_o^x]$ clusters are present in the (010), (100) and (011) surfaces. Therefore, the top of these three surfaces has the same undercoordinated Ag clusters. The undercoordinated $[AgO_2 \cdot 4V_o^x]$ clusters are presented in the (110) and (111) surfaces and the (110) surface is also constituted by the undercoordinated $[CrO_3 \cdot V_o^x]$ clusters. The D_b calculated shows a structural disorder at the top of surface, i.e., a higher D_b value indicates a higher value of broken bonds on the surface, while smaller D_b values indicate a local order at the surface, less undercoordinated cluster with neutral oxygen vacancy. Therefore, the D_b values follow the order: (001) < (111) < (110) < (010) < (011) < (100) < (101), with values of 8.45, 14.00, 15.71, 15.79, 17.39, 17.72, and 22.00 nm^{-2}, respectively. These results indicated that the (001) and (101) surfaces are the most and less organized surfaces with E_{surf} of 1.70 J/m^2 and 1.41 J/m^2, respectively.

3.2. Photocatalytic Tests

The photocatalytic activity of Ag_2CrO_4 samples were tested for the degradation of RhB under visible light irradiation. The RhB shows the characteristic absorption peak located at 554 nm, relative to its conjugated chromophore xanthene ring [43], which due to the action of light undergoes a hypochromic displacement of the absorption as result of the de-ethylation of the N,N'-diethylammonium functional groups [44]. The photodegradation results are shown in **Fig. 7** and **Fig. 8** by variations of RhB concentration (C_n/C_0) as function of irradiation time, being C_n and C_0 the concentration at a time *t* and the initial concentration, respectively.

Fig. 7. UV-vis absorption spectra of the RhB aqueous solution in the presence of Ag_2CrO_4 powders, obtained by the CP method with H_2O as a solvent at A) 30, B) 60 and C) 90 °C and with NH_3 as a solvent at D) 30, E) 60 and F) 90 °C.

Since most of the heterogeneous photocatalytic mechanisms for semiconductors are considered as pseudo-first order reaction due to low initial concentration of dye and the constant concentration of catalyst [45,46], the Langmuir-Hinshelwood (L-H) model [47] was used according to **equation 1**. In this equation, *k* is the rate constant and *t* the reaction time. Therefore, if the reaction order is of pseudo-first order, the plot of ln

C_0/C_n in function of irradiation time gives a straight line in which the angular coefficient is the *k* value. The L-H plots were performed in order to verify the reaction order and to obtain the rate constant for all samples, as shown in **Fig. 8C-D**.

$$ln\frac{C_0}{C_n} = kt \quad (1)$$

Fig. 8. A) Relative concentration of RhB dye (C/C_0) versus time (min) of Ag_2CrO_4 powders obtained by CP method with H_2O as a solvent at different temperatures and B) with NH_3 as a solvent. (C) Reaction kinetics of RhB degradation $\ln(C_0/C_n)$ versus *t* (min) for of Ag_2CrO_4 powders and D) with NH_3 addition. E) Efficiency of degradation (%) of RhB dye under exposure to UV-vis radiation, in the presence of Ag_2CrO_4 and different scavengers for the both samples synthesized at 60 °C.

It can be observed that RhB underwent faster degradation in the presence of Ag_2CrO_4 prepared at 60 °C with H_2O, and the same with NH_3 compared to other temperatures, with 59 and 24% of degradation in one hour of reaction, respectively (**Fig. 8A-B**). For comparison, when RhB solution was subjected to visible light irradiation without the samples, *i.e.* photolysis test, under the same experimental conditions, practically no degradation was observed. As expected, the samples synthesized at 60 °C in H_2O and NH_3 presented a higher rate constant in relation to the other samples, with *k* = 0.0126 and 0.0037, respectively (**Fig. 8C-D**). The photocatalytic mechanisms for all samples were well fitted as pseudo-first order reaction, which agrees with literature data [48–50].

On the whole, it can be observed that in the crystals obtained in NH_3 medium there is a preference by the exposition of the surfaces rich in low-coordinated Ag atoms and exposed coordinated Cr atoms (**Fig. 6 and Table 1**). In the same way, the higher photocatalytic activity of the species obtained at 60 °C may be associated with the exposition of the undercoordinated Ag rich facets. As aforementioned, the (011) surface is exposed in both morphologies 2 and 5 (obtained in H_2O and in NH_3, respectively), which is composed by $[AgO_2 \cdot 4V_o^x]$, $[AgO_3 \cdot 3V_o^x]$ and $[CrO_4]$ clusters, accomplished by the (010) and (110) surfaces and by the (001) and (111) surfaces, respectively. According to **Table 1**, these surfaces in addition to the (101) surface have the largest number of $[AgO_3 \cdot 3V_o^x]$ clusters (**Fig. 6**). In this sense, the correlation between the theoretical models and the experimental data suggest that the photocatalytic activity may be associated to the presence of these crystalline planes in the final morphologies, demonstrated that the photocatalytic activity of Ag_2CrO_4 crystals is surface-dependent.

In majority of these surfaces, the Ag and O atoms are in the $[AgO_3 \cdot 3V_o^x]$ clusters in a planar configuration with small RMSD (Root-Mean-Square Deviation) (less than 0.1 Å) with two angles around 90° and one close to 180°. This configuration can be seen as a residual geometry of the octahedral [AgO_6] clusters. In this arrangement the Ag cations are exposed and they are capable to interact with electron donor species. Comparatively, the Ag formal oxidation state in bulk is +0.78 while in the (011) surface it varies from +0.59 to +0.75. The presence of these reduced Ag atoms in the surface might act as a driving force to improve the photocatalytic activity.

As previously described, both samples obtained with H_2O and NH_3 solvents at 60 °C presented higher photodegradation activity compared to samples obtained in 30 and 90 °C. Due to these results, photocatalytic experiments using scavengers' reagents were performed for these two samples in order to understand the photodegradation mechanism. Tert-butyl alcohol (TBA), silver nitrate (SN), p-benzoquinone (BQ), and ammonium oxalate (AO) were used as scavengers for hydroxyl radical (OH^*), electron (e'), superoxide radical (O_2'), and hole ($h^\bullet$), respectively. **Fig. 8E** shows the photodegradation efficiency of samples obtained with H_2O and NH_3 with and without scavengers. As can be seen, the experiments using BQ and AO for both samples obtained with H_2O and NH_3, i.e. the absence of superoxide and holes for reactions, presented lower photodegradation efficiency compared to others charge carriers and reactive oxygen species (ROS). Therefore, we can conclude that the O_2' and $h^\bullet$ are the main responsible for photodegradation reactions in both samples.

As observed by the results of Rietveld refinements of these samples (see section *A* of the SI), the clusters that compose the structure of obtained Ag_2CrO_4 with higher structural distortions were octahedral [AgO_6], while both tetrahedral [AgO_4] and [CrO_4] clusters presented structural order at short-range. Considering that the ordering degree of cluster is directly associated to local symmetry, these distorted and ordered clusters correspond to asymmetric and symmetric clusters, respectively. Furthermore, the electronic bands structure by partial DOS indicates that the top of VB of Ag_2CrO_4 is mainly composed of Ag 4*d* and O 2*p* orbitals, while the bottom of CB is mainly composed of Cr 3*d* and O 2*p* orbitals (see section *C* of the SI). Therefore, the structural composition of top of VB is mainly formed by [AgO_6] clusters while the bottom of CB is composed by the [CrO_4] clusters. Besides, it was shown in the analysis of the surfaces

that there are undercoordinated Ag atoms with oxygen vacancies and completed coordinated Cr atoms on the top of the surfaces that composed the crystal morphologies.

From these results, it is possible to propose a photodegradation mechanism, as given by **equations 2-6**, which were constructed using Kröger-Vink notation [42]:

$$[CrO_4]^x + [AgO_3 \cdot 3V_o^x] \rightarrow [CrO_4]' + [AgO_3 \cdot 3V_o^\bullet] \quad (2)$$

$$[AgO_3 \cdot 3V_o^\bullet] + H_2O \rightarrow [AgO_3 \cdot 3V_o^x] + OH^* + H^\bullet \quad (3)$$

$$[CrO_4]' + O_2 \rightarrow [CrO_4]^x + O_2' \quad (4)$$

$$O_2' + H^\bullet \rightarrow O_2H^* \quad (5)$$

$$OH^* + O_2H^* + RhB \rightarrow CO_2 + H_2O + degradation\ products \quad (6)$$

where the ($'$), ($\bullet$), (x) sub-index mean negative, positive and neutral chargers, respectively, in the Kröger-Vink notation.

As can be seen above, the Ag and Cr clusters generate a polarization of the electron density, leading to formation of electrons in pre-excited states [51,52]. These electrons can interact with neutral neighbors $[CrO_4]^x$ and $[AgO_3 \cdot 3V_o^x]$ clusters, resulting in a charge transfer between these clusters and then forming negatively and positively charged $[CrO_4]'$ and $[AgO_3 \cdot 3V_o^\bullet]$ clusters, respectively. The positively charged $[AgO_3 \cdot 3V_o^\bullet]$ clusters are considered to keep the hole, which is well known that can easily oxidizes the H_2O molecules in contact with the surface, generating OH^* and a proton ($H^\bullet$) [4,53]. The negatively $[CrO_4]'$ clusters in the CB can promote the reduction reaction of dissolved O_2 to form the O_2'. This radical reacts with the proton released in **equation 5** to produce the hydroperoxyl radical (O_2H^*), which is one of the most reactive species generated in the photodegradation mechanism [4,54]. Therefore, the holes, i.e. $[AgO_3 \cdot 3V_o^\bullet]$, play a key role along the reaction mechanism since they are responsible for production of $H^\bullet$ and also the OH^* radical. In addition, the O_2' radical plays also a crucial role to reaction mechanism since they react with protons to produce a highly reactive species, the O_2H^* radical. Herewith, a quenching process involving holes and O_2' radicals directly hinders the production of O_2H^* radicals due to absence of the reactants in **equation 5**, thus drastically reducing the photodegradation efficiency in the **equation 6**.

3.3. Microbiological and cellular viability tests

Biofilms of *C. glabrata* present a reduction of the susceptibility to antifungals commonly used, in comparison to the planktonic form [55]. These species are naturally resistant to various antifungal and host protective molecules [56], making its elimination even more difficult. In this way, the development of new antifungal agents for its elimination becomes very important.

The colony forming units of *C. glabrata* after exposure to different concentrations of Ag_2CrO_4 are shown in **Fig. 9A**. It can be observed that all the samples were able to eliminate *C. glabrata*. The material that presented the highest antifungal activity was Ag_2CrO_4 prepared at 60 °C with water. A concentration of 0.24 μg/mL of this material avoided the growth of *C. glabrata*. It is widely known that silver is a powerful anti-microbial agent acting against fungi [13], gram-negative and gram-positive bacteria [11], including methicillin-resistant *Staphylococcus aureus* (MRSA), a highly pathogenic species responsible for severe nosocomial infections [57]. In our case, for the samples that presented the highest minimum fungicidal concentration (MFC), the values are lower than those reported by other materials associated with silver [58,59].

The viability of L929 cells exposed to different sample for 24h at different concentrations were evaluated. The results showed that the cellular viability (> 80%) was high to concentrations below 1.5 μg/mL independently of the material (**Fig. 9B**). However, the Ag_2CrO_4-NH_3 30°C and Ag_2CrO_4-NH_3 60 °C at low levels (~5 μg/mL) presented a high cytotoxicity that was able to drop the cellular viability to levels below to 50%. In contrast, Ag_2CrO_4 30 °C, Ag_2CrO_4 60 °C and Ag_2CrO_4-NH_3 90°C showed elevated level of cytotoxicity only at concentrations above of 18 μg/mL, being approximately 5-fold less cytotoxic than the previous types of materials. In relation to Ag_2CrO_4 90 °C, the level of its cytotoxicity was intermediary in comparison with the two previous groups.

Fig. 9. A) *Candida glabrata* growth as a function of different concentrations of Ag_2CrO_4. B) Cellular viability of L929 cells exposed to Ag_2CrO_4 obtained by CP method with H_2O and NH_3 as a solvent.

Silver nanoparticles and silver-based materials are widely studied in biological and biomedical fields, such as antibacterial [60–62], antifungal [59,63,64] and anticancer therapeutics [65]. However, its cytotocixity can make its application unfeasible. In this study, it is possible to observe that for all samples, the cells showed high viability

(above 70%) when treated with the concentrations of greater antifungal activity (**Fig. 9B**).

Studies have shown that the use of chromium-based materials may accumulate in some organisms [66] and present a wide range of lethal effects [67]. Wise et al. [68] demonstrated that exposure of cultured cells to chromate samples was able to induce cell death, cause chromosomal aberrations and double-strand breaks of the genetic material. In humans, chromate is reported to be a highly genotoxic agent [69]. Its insoluble form in water results in the partial dissolution of the sample in the extracellular environment, releasing Cr ions, and the toxic effects resulting from the uptake and intracellular reduction of Cr (VI) to Cr (III) ions. Genotoxic effects may cause carcinogenic, teratogenic and developmental problems.

In an attempt to minimize the effects of the exposure of chromate to biological systems, several methods of synthesis are studied. In this work, we can observe that Ag_2CrO_4–NH_3 90°C presented lower cytotoxicity power than the other samples, showing that in some way, its characteristics can minimize the effects caused to the cells.

The mechanism of action is related to the production of ROS, through the interaction of the undercoordinated clusters present in the morphology with the H_2O and O_2 molecules. The ROS in contact with the microorganism causes membrane damage and death [8]. In this study, the release of ROS can be proven by the photodegradation tests with the presence of scavengers, where we can assume that both O_2' and $h^{\bullet}$ species are key in the antifungal activity. At nanoscale, the surface atoms and structural defects increase, the active sites at the exposed surfaces exponentially increase to be capable to churn out a plethora of ROS and provoke oxidative stress.

4. Conclusions

In summary, the surface-dependent photocatalytic (degradation of Rhodamine B), antifungal (towards *Candida glabrata*) and cellular viability (against the L929 cell line) activities of Ag_2CrO_4 microcrystals were studied in detail by combining experimental techniques and first-principles calculations. The integration of experimental results and computational modeling led to a deep insight to clarify important issues and established a theoretical base. Taking advantage of the fact that the synthesis method used in H_2O

and NH_3 has allowed to obtain samples with homogeneous morphologies, herein, we have systematically investigated, for the first time, both the surface characteristics and electronic structures of Ag_2CrO_4 microcrystals with different exposed surfaces and morphology, which were prepared by the co-precipitation method. The variations in structure and electronic properties were monitored by XRD with Rietveld refinements, micro-Raman and UV-vis spectroscopies, and photoluminescence emissions, while surface morphology were characterized by FE-SEM images. To obtain a wide variety of crystal morphologies, the surface chemistry, i.e., the relative stability of the faceted crystals was tuned. Samples obtained with H_2O and NH_3 solvents at 60 °C presented higher photodegradation activity, and the superoxide radical and holes are the main responsible for photodegradation reactions in both samples.

Present experimental and theoretical work has highlighted several key parameters (surface dependent) that determine the photocatalytic, antifungal and cytotoxicity of Ag_2CrO_4 microcrystals and provided some general principles for material design. Different activities can be associated to the different number of superficial undercoordinated Ag atoms. Presence of (011) surface with a larger amount of undercoordinated Ag clusters, like $[AgO_3 \cdot 3V_o^x]$, and $[AgO_6]$ and $[CrO_4]$ clusters that formed the Ag_2CrO_4 morphologies is the key factor that can rationalize both the photocatalytic, antifungal and cytotoxicity activities.

We have demonstrated a new approach to understand the role of the Ag_2CrO_4 crystal surfaces, which also has great potential for addressing many fundamental issues in related materials. We believe that our results offer new insights regarding the local coordination of superficial Ag and Cr cations (i.e., clusters) on each exposed surface of the corresponding morphology, that dictate these properties, a field that has so far remained unexplored.

Our study illustrates the enormous potential of surface oriented Ag_2CrO_4, confirming that DFT calculations combined with experimental evidence play a fundamental role not only to obtain a number of crystal morphologies, that may offer improved performance, but also these insights can contribute to the rational design of new materials for multifunctional applications.

Declaration of Competing Interest

The authors declare that they have no known competing financial interests or personal relationships that could have appeared to influence the work reported in this paper.

Acknowledgments

This work was funded in part by Fundação de Amparo à Pesquisa do Estado de São Paulo - FAPESP (2013/07296-2; 2016/23891-6; 2017/12594-3; 2017/12594-3; 2019/01732-1; 2019/13507-2), FINEP, Conselho Nacional de Desenvolvimento Cientifico e Tecnológico - CNPq (166281/2017-4), and CAPES. This work used computational resources of the "Centro Nacional de Processamento de Alto Desempenho em São Paulo" (CENAPAD-SP), "Centro de Computação John David Rogers" (CCJDR-UNICAMP), and the CENAPAD-RJ (SDumont). J.A. acknowledges Universitat Jaume I (project UJI-B2019-30), and the Ministerio de Ciencia, Innovación y Universidades (MICIU) (project PGC2018094417-B-I00) for financially supporting this research. I. S. thanks the Spanish Ministerio de Economía, Industria y Competitividad (MINECO) for a postdoctoral "Juan de la Cierva-Incorporación" fellowship (IJCI-2016-30590), and the financial support from MICIU through the "José Castillejo" Mobility Program (CAS19/00339).

Appendix A. Supplementary material

Supplementary data to this article can be found online.

References

[1] J. Tang, J. Ye, Correlation of crystal structures and electronic structures and photocatalytic properties of the W-containing oxides, J. Mater. Chem. 15 (2005) 4246–4251. doi:10.1039/b504818d.

[2] Y.V.B. De Santana, J.E.C. Gomes, L. Matos, G.H. Cruvinel, A. Perrin, C. Perrin, J. Andrés, J.A. Varela, E. Longo, Silver molybdate and silver tungstate nanocomposites with enhanced photoluminescence, Nanomater. Nanotechnol. 4 (2014) 22–31. doi:10.5772/58923.

[3] Z. Lin, J. Li, Z. Zheng, J. Yan, P. Liu, C. Wang, G. Yang, Electronic Reconstruction of α-Ag_2WO_4 Nanorods for Visible-Light Photocatalysis, ACS Nano. 9 (2015) 7256–7265. doi:10.1021/acsnano.5b02077.

[4] R.A. Roca, J.C. Sczancoski, I.C. Nogueira, M.T. Fabbro, H.C. Alves, L. Gracia,

L.P.S. Santos, C.P. De Sousa, J. Andrés, G.E.L. Jr, E. Longo, L.S. Cavalcante, Facet-dependent photocatalytic and antibacterial properties of α-Ag_2WO_4 crystals: combining experimental data and theoretical insights, Catal. Sci. Technol. 5 (2015) 4091–4107. doi:10.1039/C5CY00331H.

[5] L.F. Da Silva, A.C. Catto, W.A. Jr, L.S. Cavalcante, J. Andrés, K. Aguir, V.R. Mastelaro, E. Longo, A novel ozone gas sensor based on one-dimensional (1D) α-Ag_2WO_4 nanostructures, Nanoscale. 6 (2014) 4058–4062. doi:10.1039/c3nr05837a.

[6] B. Arslan Hamat, M.K. Aydınol, Experimental investigation on the electrocatalytic behavior of Ag-based oxides, Ag_2XO_4 (X= Cr, Mo, W), for the oxygen reduction reaction in alkaline media, J. Solid State Chem. 290 (2020) 121571. doi:10.1016/j.jssc.2020.121571.

[7] C. Liang, S. Qi, S. Mingwang, W. Xianwen, W. Zhengcui, Photoswitches of One-Dimensional Ag_2MO_4 (M = Cr, Mo, and W), J. Phys. Chem. C. 113 (2009) 1764–1768. doi:10.1021/jp808907e.

[8] V.M. Longo, C.C. De Foggi, M.M. Ferrer, A.F. Gouveia, R.S. Andre, W. Avansi, C.E. Vergani, A.L. Machado, J. Andrés, L.S. Cavalcante, A.C. Hernandes, E. Longo, Potentiated electron transference in α-Ag_2WO_4 microcrystals with Ag nanofilaments as microbial agent, J. Phys. Chem. A. 118 (2014) 5769–5778.

[9] A. Beltrán, L. Gracia, E. Longo, J. Andrés, First-Principles Study of Pressure-Induced Phase Transitions and Electronic Properties of Ag_2MoO_4, J. Phys. Chem. C. 118 (2014) 3724–3732. doi:10.1021/jp4118024.

[10] A. Sreedevi, K.P. Priyanka, S.C. Vattappalam, T. Varghese, Silver Tungstate Nanoparticles for the Detection of Ethanol, Ammonia and Acetone Gases, J. Electron. Mater. 47 (2018) 6328–6333. doi:10.1007/s11664-018-6551-8.

[11] C.C. de Foggi, R.C. de Oliveira, M.T. Fabbro, C.E. Vergani, J. Andres, E. Longo, A.L. Machado, Tuning the Morphological, Optical, and Antimicrobial Properties of α-Ag_2WO_4 Microcrystals Using Different Solvents, Cryst. Growth Des. 17 (2017) 6239–6246. doi:10.1021/acs.cgd.7b00786.

[12] N.G. Macedo, A.F. Gouveia, R.A. Roca, M. Assis, L. Gracia, J. Andrés, E.R. Leite, E. Longo, Surfactant-Mediated Morphology and Photocatalytic Activity of α-Ag_2WO_4 Material, J. Phys. Chem. C. 122 (2018) 8667–8679. doi:10.1021/acs.jpcc.8b01898.

[13] C.C. Foggi, M.T. Fabbro, L.P.S. Santos, Y.V.B. de Santana, C.E. Vergani, A.L. Machado, E. Cordoncillo, J. Andrés, E. Longo, Synthesis and evaluation of α-Ag_2WO_4 as novel antifungal agent, Chem. Phys. Lett. 674 (2017) 125–129. doi:10.1016/j.cplett.2017.02.067.

[14] D. Xu, B. Cheng, J. Zhang, W. Wang, J. Yu, W. Ho, Photocatalytic activity of Ag_2MO_4 (M = Cr, Mo, W) photocatalysts, J. Mater. Chem. A. 3 (2015)

20153–20166. doi:10.1039/C5TA05248C.

[15] Y. Liu, H. Yu, M. Cai, J. Sun, Microwave hydrothermal synthesis of Ag_2CrO_4 photocatalyst for fast degradation of PCP-Na under visible light irradiation, Catal. Commun. 26 (2012) 63–67. doi:10.1016/j.catcom.2012.04.017.

[16] Y. Deng, L. Tang, G. Zeng, J. Wang, Y. Zhou, J. Wang, J. Tang, Y. Liu, B. Peng, F. Chen, Facile fabrication of a direct Z-scheme Ag_2CrO_4/g-C_3N_4 photocatalyst with enhanced visible light photocatalytic activity, J. Mol. Catal. A Chem. 421 (2016) 209–221. doi:10.1016/j.molcata.2016.05.024.

[17] J. Shen, Y. Lu, J.K. Liu, X.H. Yang, Photocatalytic activity of silver chromate materials by various synthesis methods, J. Exp. Nanosci. 11 (2016) 650–659. doi:10.1080/17458080.2015.1110624.

[18] F. Soofivand, F. Mohandes, M. Salavati-Niasari, Silver chromate and silver dichromate nanostructures: Sonochemical synthesis, characterization, and photocatalytic properties, Mater. Res. Bull. 48 (2013) 2084–2094. doi:10.1016/j.materresbull.2013.02.025.

[19] D. Xu, S. Cao, J. Zhang, B. Cheng, J. Yu, Effects of the preparation method on the structure and the visible-light photocatalytic activity of Ag_2CrO_4, Beilstein J. Nanotechnol. 5 (2014) 658–666. doi:10.3762/bjnano.5.77.

[20] W. Zhao, Y. Guo, S. Wang, H. He, C. Sun, S. Yang, A novel ternary plasmonic photocatalyst: Ultrathin g-C_3N_4 nanosheet hybrided by Ag/$AgVO_3$ nanoribbons with enhanced visible-light photocatalytic performance, Appl. Catal. B Environ. 165 (2015) 335–343. doi:10.1016/j.apcatb.2014.10.016.

[21] D. Xu, B. Cheng, S. Cao, J. Yu, Enhanced photocatalytic activity and stability of Z-scheme Ag_2CrO_4-GO composite photocatalysts for organic pollutant degradation, Appl. Catal. B Environ. 164 (2015) 380–388. doi:10.1016/j.apcatb.2014.09.051.

[22] J. Luo, X. Zhou, L. Ma, X. Xu, Rational construction of Z-scheme Ag_2CrO_4/g-C_3N_4 composites with enhanced visible-light photocatalytic activity, Appl. Surf. Sci. 390 (2016) 357–367. doi:10.1016/j.apsusc.2016.08.096.

[23] L. Shi, L. Liang, F. Wang, M. Liu, J. Sun, Ag_2CrO_4 nanoparticles loaded on two-dimensional large surface area graphite-like carbon nitride sheets: simple synthesis and excellent photocatalytic performance, Dalt. Trans. 45 (2016) 5815–5824. doi:10.1039/c5dt04644k.

[24] M. Pirhashemi, A. Habibi-Yangjeh, Ternary ZnO/AgBr/Ag_2CrO_4 nanocomposites with tandem n-n heterojunctions as novel visible-light-driven photocatalysts with excellent activity, Ceram. Int. 41 (2015) 14383–14393. doi:10.1016/j.ceramint.2015.07.072.

[25] J. Zhang, W. Yu, J. Liu, B. Liu, Illustration of high-active Ag_2CrO_4 photocatalyst

from the first-principle calculation of electronic structures and carrier effective mass, Appl. Surf. Sci. 358 (2015) 457–462. doi:10.1016/j.apsusc.2015.08.084.

[26] S. Ouyang, Z. Li, Z. Ouyang, T. Yu, J. Ye, Z. Zou, Correlation of crystal structures, electronic structures, and photocatalytic properties in a series of Ag-based oxides: $AgAlO_2$, $AgCrO_2$, and Ag_2CrO_4, J. Phys. Chem. C. 112 (2008) 3134–3141.

[27] G.S. Silva, L. Gracia, M.T. Fabbro, L.P. Serejo dos Santos, H. Beltrán-Mir, E. Cordoncillo, E. Longo, J. Andrés, Theoretical and experimental insight on Ag_2CrO_4 microcrystals: synthesis, characterization, and photoluminescence properties, Inorg. Chem. 55 (2016) 8961–8970. doi:10.1021/acs.inorgchem.6b01452.

[28] M.T. Fabbro, L. Gracia, G.S. Silva, L.P.S. Santos, J. Andrés, E. Cordoncillo, E. Longo, Understanding the formation and growth of Ag nanoparticles on silver chromate induced by electron irradiation in electron microscope: A combined experimental and theoretical study, J. Solid State Chem. 239 (2016) 220–227. doi:10.1016/j.jssc.2016.03.050.

[29] I.R. Colinas, R.C. Silva, S.R.J. Oliver, Reversible, selective trapping of perchlorate from water in record capacity by a cationic metal-organic framework, Environ. Sci. Technol. 50 (2016) 1949–1954. doi:10.1021/acs.est.5b03455.

[30] H.W. Abernathy, E. Koep, C. Compson, Z. Cheng, M. Liu, Monitoring Ag-Cr interactions in SOFC cathodes using Raman spectroscopy, J. Phys. Chem. C. 112 (2008) 13299–13303.

[31] S.W. Sofie, P. Gannon, V. Gorokhovsky, Silver-chromium oxide interactions in SOFC environments, J. Power Sources. 191 (2009) 465–472. doi:10.1016/j.jpowsour.2009.02.036.

[32] R.F. Alamdari, S.S. Hajimirsadeghi, I. Kohsari, Synthesis of Silver Chromate Nanoparticles: Parameter Optimization Using Taguchi Design 1, Inorg. Mater. 46 (2010) 60–64. doi:10.1134/S0020168510010140.

[33] D. Santamaría-Pérez, E. Bandiello, D. Errandonea, J. Ruiz-Fuertes, O. Gomis, J.A. Sans, F.J. Manjón, P. Rodríguez-Hernández, A. Muñoz, Phase behavior of Ag_2CrO_4 under compression: Structural, vibrational, and optical properties, J. Phys. Chem. C. 117 (2013) 12239–12248. doi:10.1021/jp401524s.

[34] A.K. Kushwaha, Uğur, S. Akbudak, G. Uğur, Investigation of structural, elastic, electronic, optical and vibrational properties of silver chromate spinels: Normal ($CrAg_2O_4$) and inverse (Ag_2CrO_4), J. Alloys Compd. 704 (2017) 101–108. doi:10.1016/j.jallcom.2017.02.055.

[35] K. Qi, R. Selvaraj, L. Wang, Editorial: Functionalized Inorganic Semiconductor Nanomaterials: Characterization, Properties, and Applications, Front. Chem. 8 (2020) 1–3. doi:10.3389/fchem.2020.616728.

[36] R. Marschall, Semiconductor Composites: Strategies for Enhancing Charge Carrier Separation to Improve Photocatalytic Activity, Adv. Funct. Mater. 24 (2014) 2421–2440. doi:10.1002/adfm.201303214.

[37] H. Huan, H. Jile, Y. Tang, X. Li, Z. Yi, X. Gao, X. Chen, Fabrication of ZnO@Ag@Ag_3PO_4 Ternary Heterojunction: Superhydrophilic Properties, Antireflection and Photocatalytic Properties, Micromachines. 11 (2020) 309.

[38] K. Momma, F. Izumi, VESTA 3 for three-dimensional visualization of crystal, volumetric and morphology data, J. Appl. Crystallogr. 44 (2011) 1272–1276. doi:10.1107/S0021889811038970.

[39] J. Andrés, L. Gracia, A.F. Gouveia, M.M. Ferrer, E. Longo, Effects of surface stability on the morphological transformation of metals and metal oxides as investigated by first-principles calculations, Nanotechnology. 26 (2015) 405703. doi:10.1088/0957-4484/26/40/405703.

[40] M.M. Ferrer, A.F. Gouveia, L. Gracia, E. Longo, J. Andrés, A 3D platform for the morphology modulation of materials: First principles calculations on the thermodynamic stability and surface structure of metal oxides: Co_3O_4, α-Fe_2O_3, and In_2O_3, Model. Simul. Mater. Sci. Eng. 24 (2016) 025007. doi:10.1088/0965-0393/24/2/025007.

[41] A.F. Gouveia, M.M. Ferrer, J.R. Sambrano, J. Andrés, E. Longo, Modeling the atomic-scale structure, stability, and morphological transformations in the tetragonal phase of $LaVO_4$, Chem. Phys. Lett. 660 (2016) 87–92. doi:10.1016/j.cplett.2016.08.013.

[42] F.A. Kröger, H.J. Vink, Relations between the concentrations of imperfections in crystalline solids, J. Phys. Chem. Solids. 5 (1958) 208–223. doi:10.1016/0022-3697(58)90069-6.

[43] X. Zhao, Y. Zhu, Synergetic degradation of rhodamine B at a porous $ZnWO_4$ film electrode by combined electro-oxidation and photocatalysis, Environ. Sci. Technol. 40 (2006) 3367–3372. doi:10.1021/es052029e.

[44] P.F.S. Pereira, A.F. Gouveia, M. Assis, R.C. De Oliveira, I.M. Pinatti, M. Penha, L. Gracia, J. Andre, E. Longo, $ZnWO_4$ nanocrystals: synthesis, morphology, photoluminescence and photocatalytic properties, Phys. Chem. Chem. Phys. 20 (2018) 1923–1937. doi:10.1039/c7cp07354b.

[45] N. Guettaï, H.A. Amar, Photocatalytic oxidation of methyl orange in presence of titanium dioxide in aqueous suspension. Part II : kinetics study, Desalination. 185 (2005) 439–448. doi:10.1016/j.desal.2005.04.049.

[46] B. Liu, X. Zhao, C. Terashima, A. Fujishima, K. Nakata, Thermodynamic and kinetic analysis of heterogeneous photocatalysis for semiconductor systems, Phys. Chem. Chem. Phys. 16 (2014) 8751–8760. doi:10.1039/c3cp55317e.

[47] K.V. Kumar, K. Porkodi, F. Rocha, Langmuir-Hinshelwood kinetics - A theoretical study, Catal. Commun. 9 (2008) 82–84. doi:10.1016/j.catcom.2007.05.019.

[48] K. Sorathiya, B. Mishra, A. Kalarikkal, K.P. Reddy, C.S. Gopinath, D. Khushalani, Enhancement in Rate of Photocatalysis Upon Catalyst Recycling, Sci. Rep. 6 (2016) 1–9. doi:10.1038/srep35075.

[49] X. Zhu, J. Liu, Z. Zhao, J. Yan, Y. Xu, Y. Song, H. Ji, H. Xu, H. Li, Hydrothermal synthesis of mpg-C_3N_4 and Bi_2WO_6 nest-like structure nanohybrids with enhanced visible light photocatalytic activities, RSC Adv. 7 (2017) 38682–38690. doi:10.1039/C7RA06681C.

[50] P. Li, C. Liu, G. Wu, Y. Heng, S. Lin, A. Ren, K. Lv, L. Xiao, W. Shi, Solvothermal synthesis and visible light-driven photocatalytic degradation for tetracycline of Fe-doped $SrTiO_3$, RSC Adv. 4 (2014) 47615–47624. doi:10.1039/c4ra06630h.

[51] L. Gracia, J. Andrés, V.M. Longo, J.A. Varela, E. Longo, A theoretical study on the photoluminescence of $SrTiO_3$, Chem. Phys. Lett. 493 (2010) 141–146. doi:10.1016/j.cplett.2010.05.041.

[52] M.L. Moreira, J. Andrés, L. Gracia, A. Beltrán, L.A. Montoro, J.A. Varela, E. Longo, Quantum mechanical modeling of excited electronic states and their relationship to cathodoluminescence of $BaZrO_3$, J. Appl. Phys. 114 (2013) 043714–1, 043714–9. doi:10.1063/1.4816247.

[53] X. Yue, J. Zhang, F. Yan, X. Wang, F. Huang, A situ hydrothermal synthesis of $SrTiO_3/TiO_2$ heterostructure nanosheets with exposed (001) facets for enhancing photocatalytic degradation activity, Appl. Surf. Sci. 319 (2014) 68–74. doi:10.1016/j.apsusc.2014.07.100.

[54] A.B. Trench, T.R. Machado, A.F. Gouveia, M. Assis, L.G. da Trindade, C. Santos, A. Perrin, C. Perrin, M. Oliva, J. Andrés, E. Longo, Connecting structural, optical, and electronic properties and photocatalytic activity of Ag_3PO_4:Mo complemented by DFT calculations, Appl. Catal. B Environ. 238 (2018) 198–211. doi:10.1016/j.apcatb.2018.07.019.

[55] P.K. Mukherjee, J. Chandra, *Candida* biofilm resistance, Drug Resist. Updat. 7 (2004) 301–309. doi:10.1016/j.drup.2004.09.002.

[56] L. Li, S. Redding, A. Dongari-Bagtzoglou, *Candida glabrata*, an Emerging Oral Opportunistic Pathogen, J. Dent. Res. 86 (2007) 204–215. doi:10.1177/154405910708600304.

[57] H.A. Khan, A. Ahmad, R. Mehboob, Nosocomial infections and their control strategies, Asian Pac. J. Trop. Biomed. 5 (2015) 509–514. doi:10.1016/j.apjtb.2015.05.001.

[58] D.R. Monteiro, L.F. Gorup, S. Silva, M. Negri, E.R. de Camargo, R. Oliveira, D.B. Barbosa, M. Henriques, Silver colloidal nanoparticles: antifungal effect against adhered cells and biofilms of *Candida albicans* and *Candida glabrata*., Biofouling J. Bioadhesion Biofilm Res. 27 (2011) 711–719. doi:10.1080/08927014.2011.599101.

[59] A.F. Wady, A.L. Machado, C.C. Foggi, C.A. Zamperini, V. Zucolotto, E.B. Moffa, C.E. Vergani, Effect of a silver nanoparticles solution on *Staphylococcus aureus* and *Candida spp*., J. Nanomater. 2014 (2014) 545279. doi:10.1155/2014/545279.

[60] C.C. De Foggi, R.C. de Oliveira, M. Assis, M.T. Fabbro, V.R. Mastelaro, C.E. Vergani, L. Gracia, J. Andrés, E. Longo, A.L. Machado, Unvealing the role of β-Ag_2MoO_4 microcrystals to the improvement of antibacterial activity, Mater. Sci. Eng. C. 111 (2020) 110765. doi:10.1016/j.neubiorev.2019.07.019.

[61] I.M. Pinatti, A.C.M. Tello, A.B. Trench, C.C. de Foggi, P.F.S. Pereira, M.M. Teixeira, N. Jacomaci, J. Andrés, E. Longo, Zinc-substituted Ag_2CrO_4: A material with enhanced photocatalytic and biological activity, J. Alloys Compd. 835 (2020) 155315. doi:10.1016/j.jallcom.2020.155315.

[62] L.O. Laier, M. Assis, C.C. Foggi, A.F. Gouveia, C.E. Vergani, L.C.L. Santana, L.S. Cavalcante, J. Andrés, E. Longo, Surface-dependent properties of α-Ag_2WO_4: a joint experimental and theoretical investigation, Theor. Chem. Acc. 139 (2020) 108. doi:10.1007/s00214-020-02613-z.

[63] B.N.A. da S. Pimentel, C.C. de Foggi, P.A. Barbugli, R.C. de Oliveira, E.D. de Avila, E. Longo, C.E. Vergani, Antifungal activity and biocompatibility of α-$AgVO_3$ microcrystals: A promising material against oral *Candida* disease, Mater. Sci. Eng. C. 108 (2020) 110405. doi:10.1016/j.msec.2019.110405.

[64] M.T. Fabbro, C.C. Foggi, L.P.S. Santos, L. Gracia, A. Perrin, C. Perrin, C.E. Vergani, A.L. Machado, J. Andrés, E. Cordoncillo, E. Longo, Synthesis, antifungal evaluation and optical properties of silver molybdate microcrystals in different solvents: a combined experimental and theoretical study, Dalt. Trans. 45 (2016) 10736–10743. doi:10.1039/c6dt00343e.

[65] M. Assis, T. Robeldo, C.C. Foggi, A.M. Kubo, G. Mínguez-Vega, E. Condoncillo, H. Beltran-Mir, R. Torres-Mendieta, J. Andrés, M. Oliva, C.E. Vergani, P.A. Barbugli, E.R. Camargo, R.C. Borra, E. Longo, Ag Nanoparticles/α-Ag_2WO_4 Composite Formed by Electron Beam and Femtosecond Irradiation as Potent Antifungal and Antitumor Agents, Sci. Rep. 9 (2019) 9927. doi:10.1038/s41598-019-46159-y.

[66] P. Sivaperumal, T. V. Sankar, P.G. Viswanathan Nair, Heavy metal concentrations in fish, shellfish and fish products from internal markets of India vis-a-vis international standards, Food Chem. 102 (2007) 612–620. doi:10.1016/j.foodchem.2006.05.041.

[67] A.P. Roberts, J.T. Oris, Multiple biomarker response in rainbow trout during exposure to hexavalent chromium, Comp. Biochem. Physiol. - C Toxicol. Pharmacol. 138 (2004) 221–228. doi:10.1016/j.cca.2004.08.006.

[68] J.P. Wise, S.S. Wise, C. Lacerte, J.P. Wise, A. Aboueissa, The Genotoxicity of Particulate and Soluble Chromate in Sperm Whale (*Physeter macrocephalus*) Skin Fibroblasts, Environ. Mol. Mutagen. 52 (2011) 43–49. doi:10.1002/em.20579.

[69] A.L. Holmes, S.S. Wise, J.P. Wise, Carcinogenicity of hexavalent chromium, Indian J. Med. Res. 128 (2008) 353–372. doi:10.1016/j.toxlet.2014.05.010.

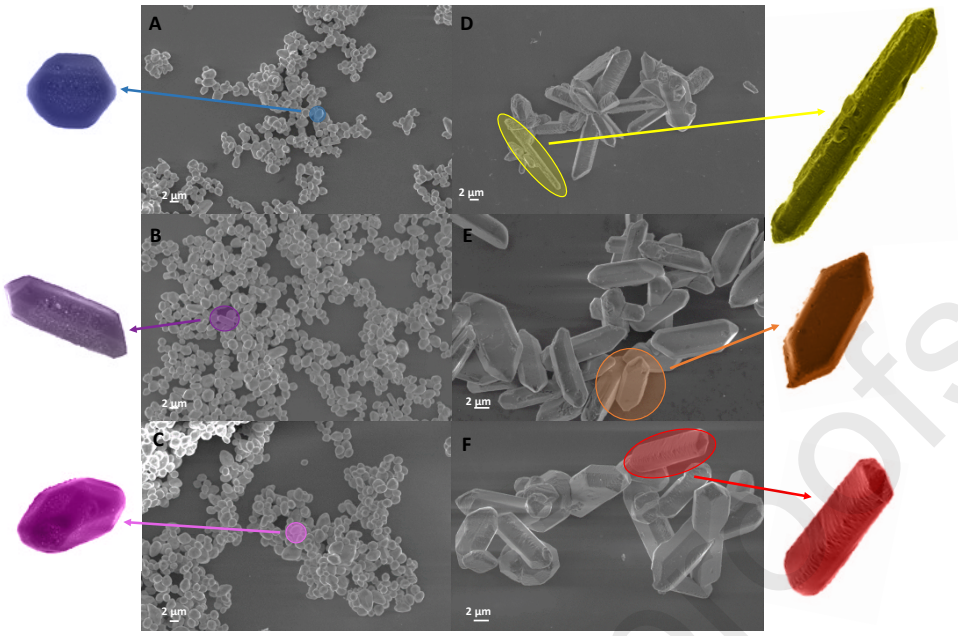

Fig. 1. FE-SEM imagens of Ag_2CrO_4 powders obtained by CP method with H_2O as a solvent at A) 30, B) 60 and C) 90 °C and with NH_3 as a solvent at D) 30, E) 60 and F) 90 °C.

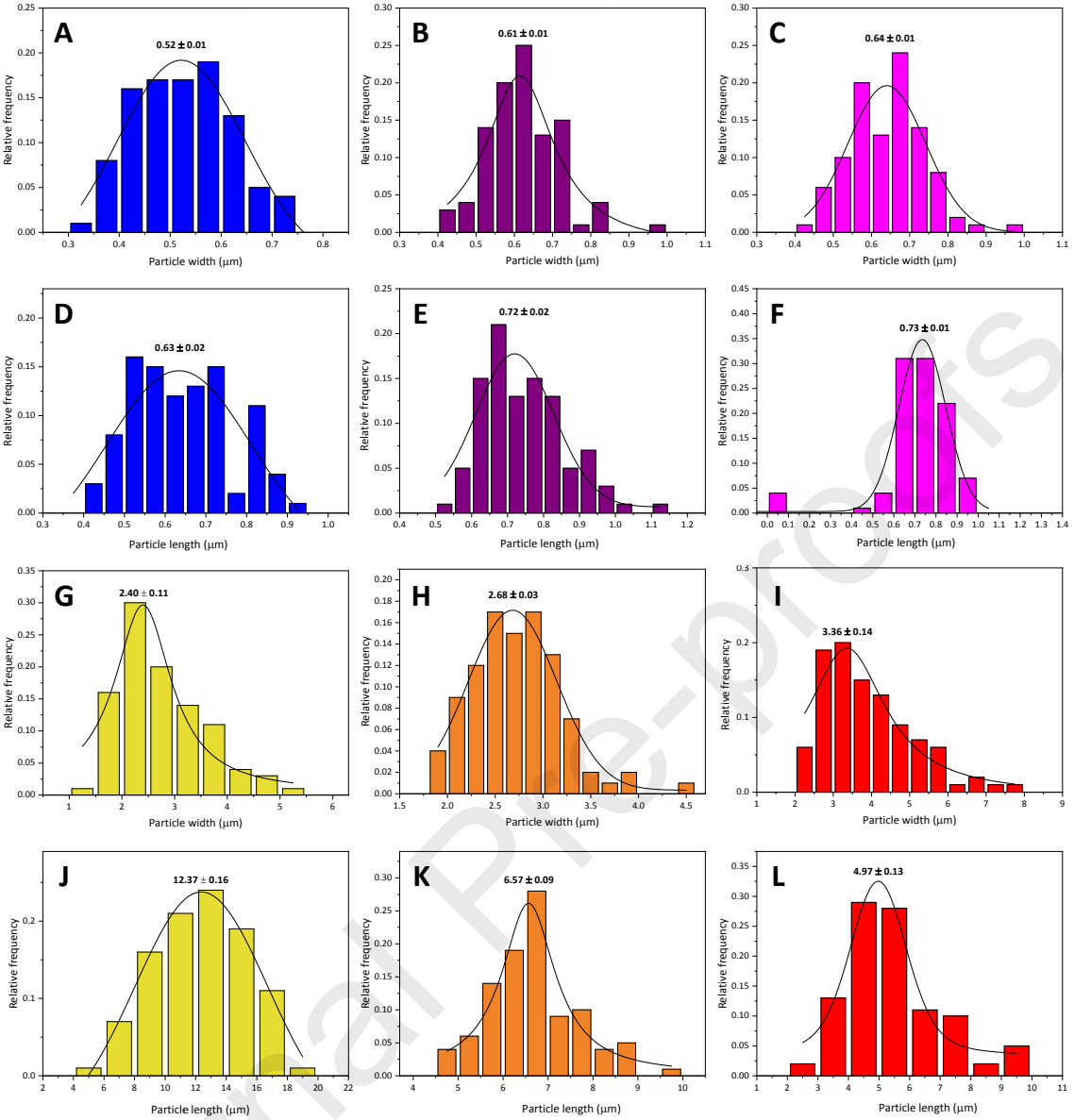

Fig. 2. Width and length distribution of Ag_2CrO_4 powders obtained by CP method with H_2O as a solvent at A-D) 30, B-E) 60 and C-F) 90 °C and with NH_3 as a solvent at G-J) 30, H-K) 60 and I-L) 90 °C.

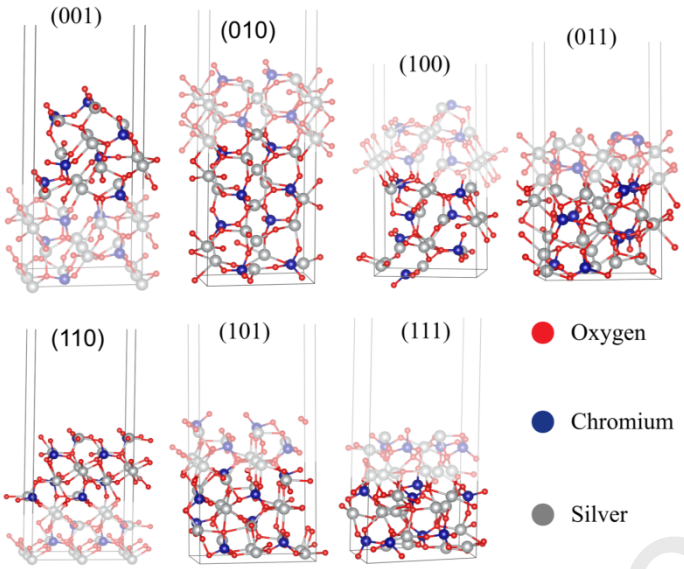

Fig. 3. Surfaces models of the Ag_2CrO_4 with their respective upper (l_1) and lower (l_2) terminations.

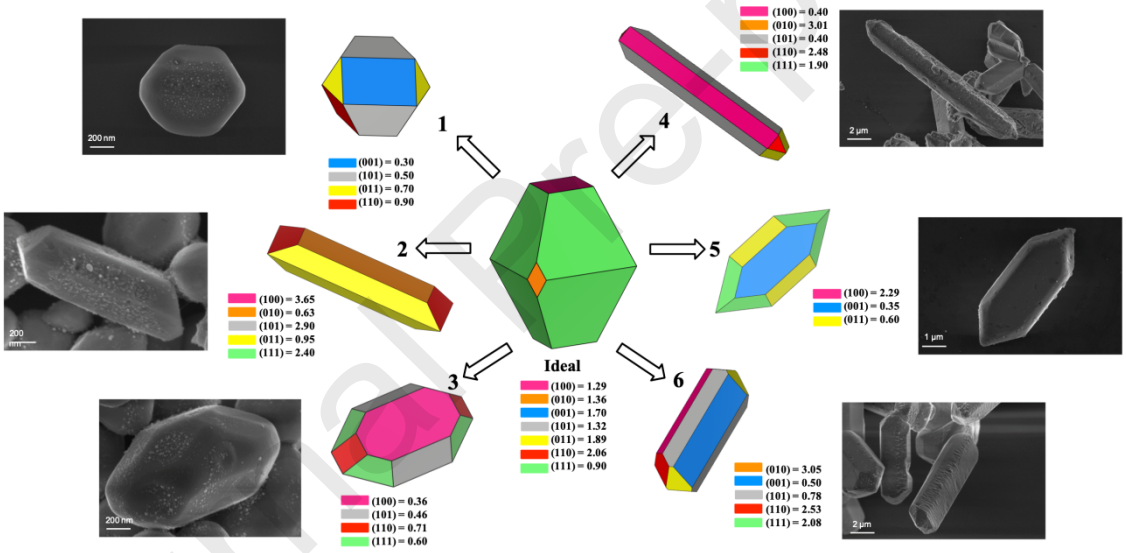

Fig. 4. Theoretical and experimental morphologies obtained by tuning the values of E_{surf} for Ag_2CrO_4. The FE-SEM imagens for each sample is inserted for comparison purposes. Surface energy value in J/m^2.

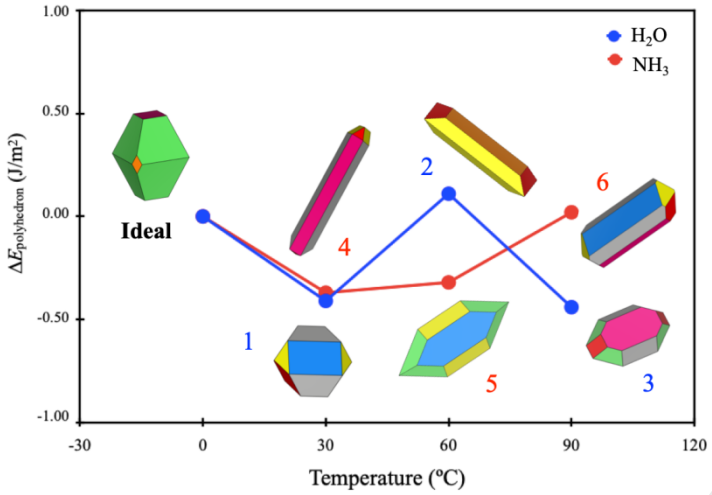

Fig. 5. Polyhedron energy profiles connecting the ideal and experimental obtained morphologies (1-6).

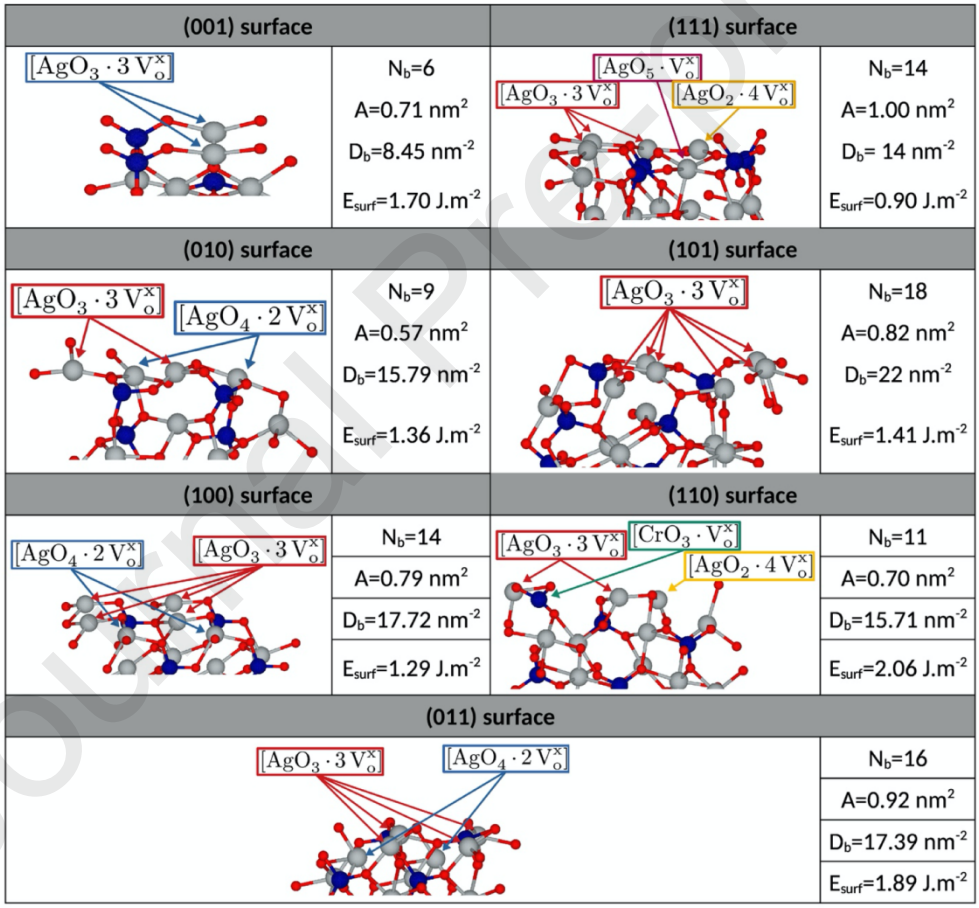

Fig. 6. Surface models for the Ag_2CrO_4 structure where the Ag and Cr clusters are highlighted. V_o^x corresponds to a neutral oxygen vacancy. The values of D_b and E_{surf} are also presented.

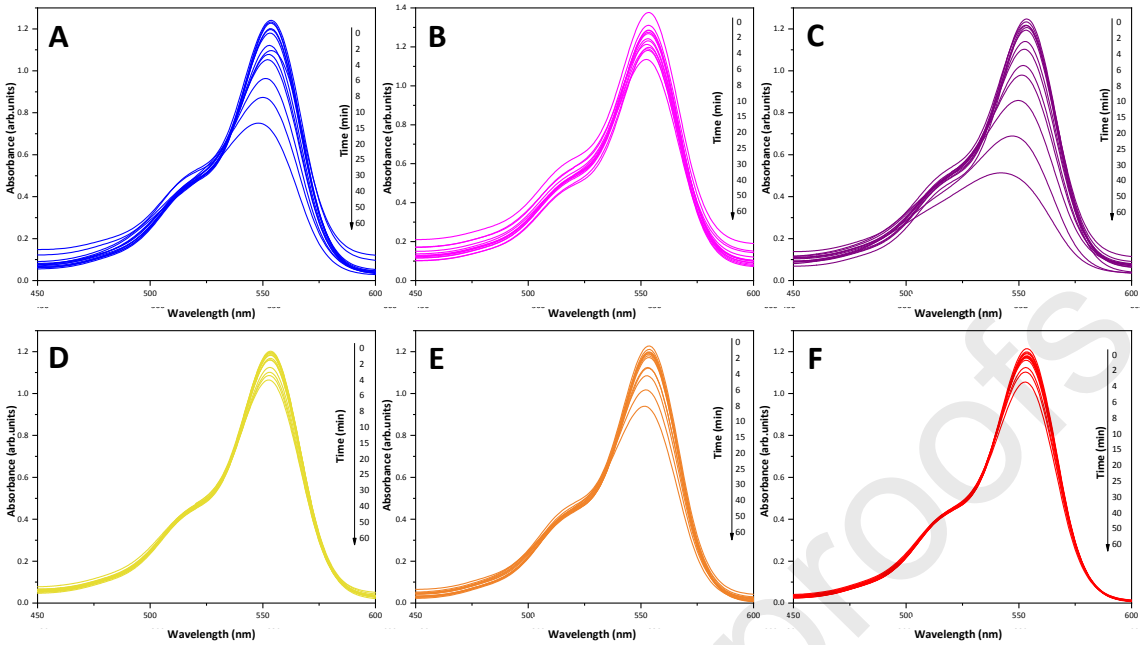

Fig. 7. UV-vis absorption spectra of the RhB aqueous solution in the presence of Ag_2CrO_4 powders, obtained by the CP method with H_2O as a solvent at A) 30, B) 60 and C) 90 °C and with NH_3 as a solvent at D) 30, E) 60 and F) 90 °C.

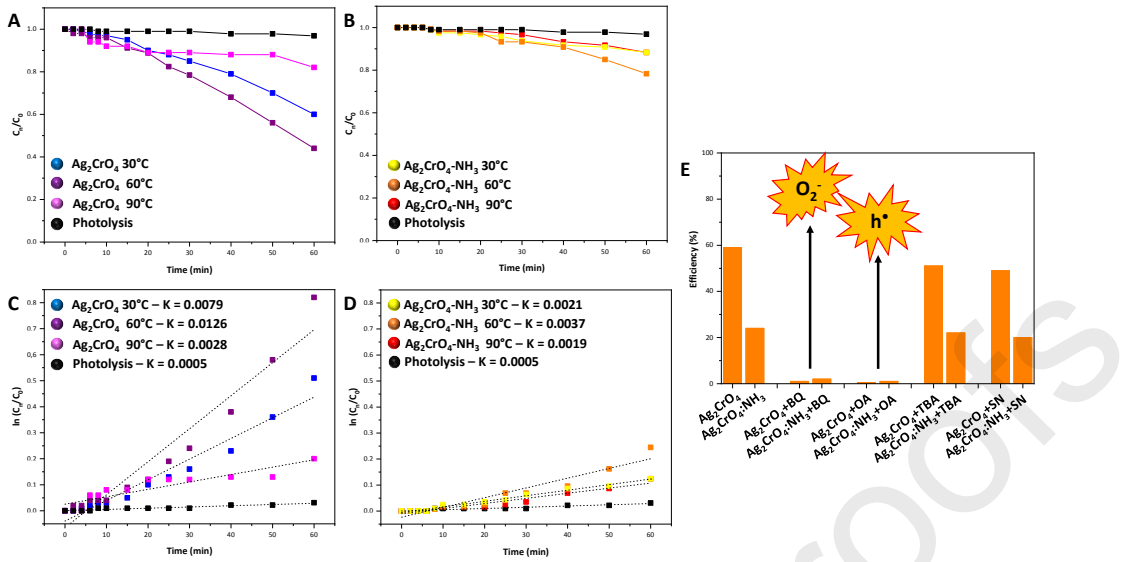

Fig. 8. A) Relative concentration of RhB dye (C/C_0) versus time (min) of Ag_2CrO_4 powders obtained by CP method with H_2O as a solvent at different temperatures and B) with NH_3 as a solvent. (C) Reaction kinetics of RhB degradation $\ln(C_0/C_n)$ versus *t* (min) for of Ag_2CrO_4 powders and D) with NH_3 addition. E) Efficiency of degradation (%) of RhB dye under exposure to UV-vis radiation, in the presence of Ag_2CrO_4 and different scavengers for the both samples synthesized at 60 °C.

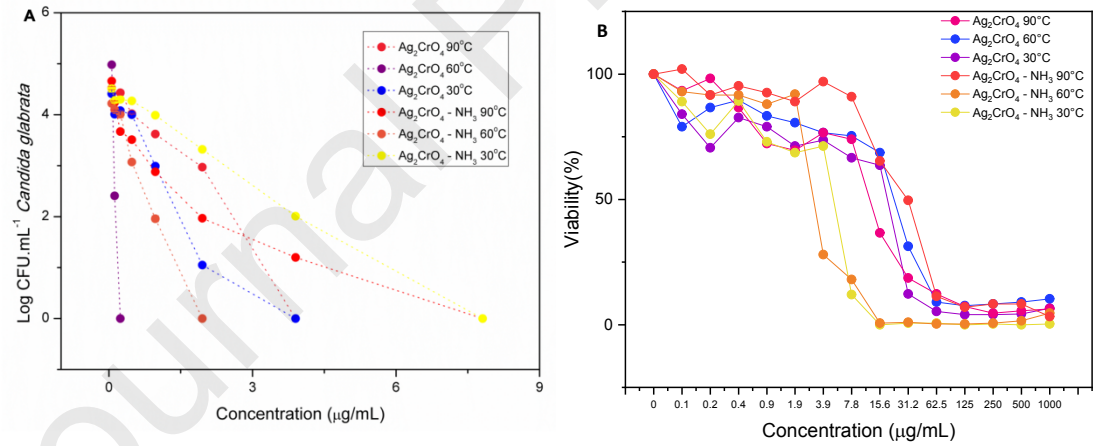

Fig. 9. A) *Candida glabrata* growth as a function of different concentrations of Ag_2CrO_4. B) Cellular viability of L929 cells exposed to Ag_2CrO_4 obtained by CP method with H_2O and NH_3 as a solvent.

Table 1. Studied surfaces, the corresponding terminations (l_i), the cleavage (E_{cut}), relaxation (E_{rel}), and surface (E_{surf}) energy values (in J/m^2), and number of atoms (NA) and their coordination number (CN) in the exposed surfaces.

Surfaces		E_{cut}	E_{rel}	E_{surf}	NA (CN)	
					Ag	Cr
(001)	l_1	2.378	-0.677	1.702	2(3)	2(4)
(001)	l_2	2.378	-0.669	1.710	3(3), 1(4), 1(5)	1(3), 1(4)
(010)	l_1	1.718	-0.265	1.453	3(4), 1(5)	2(4)
(010)	l_2	1.718	-0.354	1.364	2(4), 2(3)	2(4)
(100)	l_1	1.579	-0.175	1.404	2(4)	2(4)
(100)	l_2	1.579	-0.284	1.294	4(3), 2(4)	2(4)
(011)	l_1	2.502	-0.561	1.941	2(6), 2(3)	2(3)
(011)	l_2	2.502	-0.615	1.886	4(3), 2(4)	2(4)
(110)	l_1	3.161	-1.098	2.062	4(4),1(5)	2(4), 1(3)
(110)	l_2	3.161	-0.905	2.569	2(3), 1(2)	1(3)
(101)	l_1	1.628	-0.220	1.408	1(4), 1(3), 1(2), 1(5)	4(4)
(101)	l_2	1.628	-0.309	1.319	6(3)	2(4)
(111)	l_1	1.230	-0.186	1.045	1(3), 1(5), 1(4), 1(2)	4(4)
(111)	l_2	1.230	-0.333	0.897	3(3), 1(5), 1(2)	4(4)

Table 2. Surface energy values (E_{surf}, J/m^2), contribution of the surface area to the total area (C_i), and the polyhedron energy ($E_{polyhedron}$, J/m^2) for each crystal morphology of Ag_2CrO_4.

Morphology	Ideal		1		2		3		4		5		6	
Surface	E_{surf}	C_i	E_{surf}	C_i	E_{surf}	C_i	E_{surf}	C_i	E_{surf}	C_i	E_{surf}	C_i	E_{surf}	C_i
(100)	1.29	8.44	1.29	–	3.65	–	0.36	31.11	0.40	31.78	2.29	–	1.29	8.80
(010)	1.36	1.10	1.36	–	0.63	34.71	1.36	–	3.01	–	1.36	–	3.05	–
(001)	1.70	–	0.30	35.72	1.70	–	1.70	–	1.70	–	0.35	36.49	0.50	38.33
(101)	1.32	–	0.50	34.48	2.90	–	0.46	27.62	0.40	58.19	1.32	–	0.78	35.53
(011)	1.89	–	0.70	11.07	0.95	46.06	1.89	–	1.89	7.26	0.60	27.27	1.89	9.22
(110)	2.06	–	0.90	18.72	2.06	19.24	0.71	10.96	2.48	2.76	2.06	–	2.53	8.12
(111)	0.90	90.46	0.90	–	2.40	–	0.60	30.31	1.90	–	0.90	36.24	2.08	–
$E_{polyhedron}$	**0.94**		**0.53**		**1.05**		**0.50**		**0.57**		**0.62**		**0.96**	

Highlights

Evaluation of the surface-dependent response of Ag_2CrO_4 computational models.

Study toward unveiling the photocatalytic activity against RhB of Ag_2CrO_4.

Antifungal and cytotoxicity activities of Ag_2CrO_4 are also investigated.

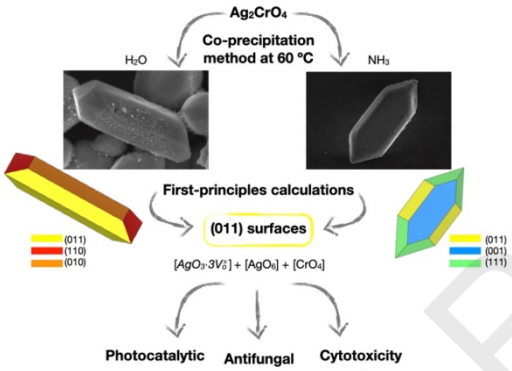

Declaration of interests

☒ The authors declare that they have no known competing financial interests or personal relationships that could have appeared to influence the work reported in this paper.

☐The authors declare the following financial interests/personal relationships which may be considered as potential competing interests:

Credit Author Statement

Marcelo Assis: Conceptualization, Methodology, Validation, Formal analysis, Investigation, Writing – original draft, Writing - review & editing, Visualization.

Camila Cristina de Foggi: Conceptualization, Methodology, Validation, Formal analysis, Investigation, Writing – original draft, Writing - review & editing, Visualization.

Vinicius Teodoro: Conceptualization, Methodology, Validation, Formal analysis, Investigation, Writing – original draft, Writing - review & editing, Visualization, Project administration, Funding acquisition.

João Paulo de Campos da Costa: Conceptualization, Methodology, Validation, Formal analysis, Investigation, Writing – original draft, Writing - review & editing, Visualization.

Carlos Eduardo Silva: Conceptualization, Methodology, Validation, Formal analysis, Investigation, Writing – original draft, Writing - review & editing, Visualization, Project administration, Funding acquisition.

Thaiane Robeldo: Conceptualization, Methodology, Validation, Formal analysis, Investigation, Writing – original draft, Writing - review & editing, Visualization.

Priscila Fernanda Caperucci: Conceptualization, Methodology, Validation, Formal analysis, Investigation, Writing – original draft, Writing - review & editing, Visualization.

Carlos Eduardo Vergani: Resources, Writing – original draft, Writing - review & editing, Visualization, Project administration, Funding acquisition.

Ricardo Carneiro Borra: Investigation, Resources, Writing – original draft, Writing - review & editing, Visualization, Project administration, Funding acquisition.

Ivan Sorribes: Conceptualization, Methodology, Validation, Formal analysis, Investigation, Writing – original draft, Writing - review & editing, Visualization, Project administration, Funding acquisition.

Amanda Fernandes Gouveia: Methodology, Validation, Formal analysis, Investigation, Writing – original draft, Writing - review & editing, Visualization.

Miguel A. San-Miguel: Conceptualization, Investigation, Resources, Writing – original draft, Writing - review & editing, Visualization, Project administration, Funding acquisition.

Juan Andrés: Conceptualization, Investigation, Resources, Writing – original draft, Writing - review & editing, Visualization, Project administration, Funding acquisition.

Elson Longo: Conceptualization, Investigation, Resources, Writing – original draft, Writing - review & editing, Visualization, Project administration, Funding acquisition.